Ligand exchange provides new insight into the role of humic substances in the marine iron cycle

Sukekava, Camila F.; Downes, Javier; Filella, Montserrat; Vilanova, Bartolomé; Laglera, Luis M.

How to cite

SUKEKAVA, Camila F. et al. Ligand exchange provides new insight into the role of humic substances in the marine iron cycle. In: Geochimica et cosmochimica acta, 2024, vol. 366, p. 17–30. doi: 10.1016/j.gca.2023.12.007

This publication URL: https://archive-ouverte.unige.ch/unige:173838

Publication DOI: 10.1016/j.gca.2023.12.007

Geochimica et Cosmochimica Acta 366 (2024) 17–30

Contents lists available at ScienceDirect

Geochimica et Cosmochimica Acta

journal homepage: www.elsevier.com/locate/gca

Ligand exchange provides new insight into the role of humic substances in the marine iron cycle

Camila F. Sukekava [a,b], Javier Downes [a], Montserrat Filella [c], Bartolomé Vilanova [a], Luis M. Laglera [a,d,*]

[a] Departamento de Química, University of the Balearic Islands, Palma, Balearic Islands 07122, Spain
[b] Instituto de Oceanografia, Fundação Universidade Federal do Rio Grande, Rio Grande 96203900, Brazil
[c] Department F.-A. Forel, University of Geneva, Boulevard Carl-Vogt 66, CH-1205 Geneva, Switzerland
[d] Laboratori Interdisciplinar sobre Canvi Climátic, University of the Balearic Islands, Palma, Balearic Islands 07122, Spain

ARTICLE INFO

Associate editor: Yoshiki Sohrin

Keywords:
Humic substances
Iron speciation
Iron cycling
Ligand exchange
Siderophores

ABSTRACT

Organic complexation of iron plays a crucial role in preventing its precipitation, facilitating its transport, and modulating its reactivity and bioavailability in natural waters. Although humic substances (HS) complexes serve as the primary source of terrestrial iron reaching ocean waters, the transition from Fe-HS species to other forms of organic complexation with ocean autochthonous ligands has not yet been properly described. Taking advantage of the electrolability of Fe-HS complexes, we monitored the ligand exchange of iron-saturated Suwannee River fulvic and humic acids (SRFA and SRHA) after the addition of desferrioxamine B (DFOB) and other ligands for comparison. We observed that Fe-HS concentrations gradually decreased until reaching an apparent steady state, typical of a reversible reaction within 1 to 15 h. The dissociation kinetics and species partitioning of Fe-SRHS complexes at the equilibrium showed some features contrary to the current paradigm of HS iron complexation. The affinity of SRFA to bind iron is close to that of DFOB and for SRHA is even higher. The heterogeneity of the HS iron binding groups was confirmed, although experiments in NaCl solutions revealed that in seawater it is substantially caused by the interaction of major divalent ions. The different dissociation kinetics of Fe-SRHS complexes obtained with different competing ligands and the absence of Fe-DFOB dissociation in the presence of iron-free SRFA indicate an intimate associative mechanism of ligand exchange, with the presence of a ternary complex (SRHS-Fe-DFOB) that does not form if the departing complex is Fe-DFOB. We hypothesize that at the concentrations of HS and siderophores found in the open ocean, iron ligand exchange is limited and organic iron speciation will be close to being regulated on a "first come, first served" basis. Experiments conducted under saturation of all iron complexes support the formation of a permanent concentration of a ternary complex. Our findings show the real complexity of cation-ligand interactions in seawater, with implications for the interpretation of recent chromatographic and electrochemical measurements and for the understanding of iron partitioning in the presence of ubiquitous HS.

1. Introduction

Organic complexation is the key process in regulating iron concentration, transport, reactivity and bioavailability in the ocean (Gledhill and Buck, 2012). Due the high biological requirements of marine organisms for iron and the very limited solubility of the element in seawater (Liu and Millero, 2002), organic complexation and reduction to the more soluble Fe(II) form are paramount to ocean ecology and, subsequently, to carbon cycling. The formation of complexes with a fraction of dissolved organic matter (DOM), hereafter referred to as ligands (L), prevents the formation and aggregation of iron hydroxides and facilitates, via ligand to metal charge transfer reactions, the formation of the more bioavailable Fe(II).

HS are complex organic mixtures resulting from biological and chemical and biochemical transformations of dead plants tissues and microorganisms. HS are a physically and chemically heterogeneous mixture characterized by their hydrophobicity, a wide range of molecular sizes, and, related to the problem targeted here, the presence of a

* Corresponding author.
E-mail address: Luis.laglera@uib.es (L.M. Laglera).

https://doi.org/10.1016/j.gca.2023.12.007
Received 24 July 2023; Accepted 5 December 2023
Available online 10 December 2023

high number of cation-binding moieties (Tipping and Hurley, 1992), of which a fraction are hard bases showing a high affinity for iron (Laglera and van den Berg, 2009). HS are operationally divided into humic acids (HA) and fulvic acids (FA) depending on whether they are soluble (FA) or not (HA) at pH 1. As a result of their formation in most terrestrial and possibly marine ecosystems and their refractory character, HS are ubiquitous in natural waters, including remote areas such as the deep ocean.

Iron export from estuaries was considered irrelevant for ocean inventories due to estuarine trapping, a process caused by the aggregation and coprecipitation of terrestrial DOM, mostly composed of HS, and iron, mostly colloidal hydroxides, as the increase of the ionic strength overrides DOM repulsion electrostatic forces (Sholkovitz, 1978). This paradigm has been modified in the last two decades, leading to a common understanding that a fraction of riverine DFe is exported to the ocean as stable, and importantly, rather refractory Fe-HS complexes (Heerah and Reader, 2022; Krachler et al., 2015; Laglera and van den Berg, 2009; Muller, 2018; Oldham et al., 2017). From an ecological perspective, humic iron exports should be an important source of iron that feeds coastal blooms (Heerah and Reader, 2022; Krachler et al., 2019; Sukekava et al., 2023). Iron complexed to HS can be taken up directly by biota, but a significant fraction is expected to be sequestered by autochthonous L formed by biological processes in seawater. Although recent field studies on the interaction of HS and iron in seawater are available (Batchelli et al., 2010; Laglera et al., 2019; Laglera and van den Berg, 2009; Sukekava et al., 2023; Whitby et al., 2020a; Yang et al., 2017), the kinetics of iron ligand exchange from humic iron to other autochthonous biological ligands have not yet been described.

Most of our knowledge about the concentrations of trace element ligands in natural waters, including the calculation of the stability constant of their complexes with trace elements, comes from the use of competing ligand equilibration (CLE) with analysis by adsorptive cathodic stripping voltammetry (AdCSV) (Gerringa et al., 2014; van den Berg, 1995). The result is presented as a ligand concentration and the conditional stability constant (K') of the corresponding complex. In some cases, if the affinity of the different iron binding groups present in natural samples is grouped into classes, CLE-AdCSV can provide further insight into the heterogeneity of iron complexation by defining a stronger and a weaker ligand (L_1 and L_2, $K'_{Fe'L1} \gg K'_{Fe'L2}$). Remarkably, CLE-AdCSV techniques have failed to describe in detail the natural heterogeneity of HS binding sites (Laglera et al., 2011). During the CLE step, iron undergoes ligand exchange following competition from the added free L_{ad}. There is little information on the intimate mechanism of the reaction that regulates the kinetics (i.e, time period) before reaching the equilibrium, a period that has been described for iron in a wide range, from many minutes to nearly three days depending on the combination of natural and L_{ad} used in the experiment (Rue and Bruland, 1995; Wu and Luther III, 1995). A comprehensive summary of published kinetics and the intimate mechanisms of iron ligand exchange and their implications in CLE studies can be found elsewhere (Laglera and Filella, 2015). CLE-AdCSV studies and current speciation models are based on a number of assumptions such as the dissociative mechanism of complexes dissociation, reversibility, absence of ligand interactions with other organic components of the matrix, etc. (Gerringa et al., 2014; Stockdale et al., 2011; van den Berg, 1995).

Here we present the first CLE-CSV follow-up to equilibrium using HS as an electrolabile ligand against the competing effect of the siderophore desferroxamine B (DFOB) and other ligands commonly used in CLE experiments. This is the same process that the small fraction of terrestrial iron that survives estuarine trapping after flocculation undergoes during estuarine transition. In contrast to all previous experiments, departing and competing ligands compounds are part of natural DOM. The exchange or iron from HS complexes to biological ligands is the same process that occurs when riverine iron mixes with coastal seawater.

2. Conceptual framework

A detailed summary of the conceptual framework, including the equations that define kinetics of the dissociative (D) and associative (A) mechanisms of ligand exchange can be found in the supplementary material. For a complete overview of ligand exchange from a mechanistic point of view, we refer the reader to our previous publication on the intimate mechanism and kinetics of iron ligand exchange in seawater and its application to CLE studies (Laglera and Filella, 2015).

The iron ligand exchange of the departing complexes (Fe-HS here) caused by competition with an added ligand (L_{ad}), a situation similar to the arrival of DOM and Fe rich riverine waters to estuaries, is defined according to Eq. (1):

$$Fe-HS \; + \; L'_{ad} \; \overset{kobs}{\longleftrightarrow} \; HS' \; + \; Fe-L_{ad} \qquad (1)$$

For the interpretation of our results is important to note several concepts:

- Changes in ligand exchange kinetics with different incoming ligands are indicative of an A mechanism (Helm and Merbach, 2005).
- Some matrix components known as accelerators, mainly cations or sometimes other organics, present the ability to weaken the bond of the initial iron complex and therefore change the kinetics of Eq. (1). In the case of binding heterogeneity (like in the case of HS), each binding group reaches equilibrium after a different period, thus, the 1/[Fe-SRFA] vs. time plot lacks linear sections and as such cannot be used to study the reaction order or the existence of ternary complexes.

3. Material and methods

3.1. Apparatus

The CSV response of Fe-HS complexes was monitored in a three-electrode electrochemical cell consisting of a hanging mercury drop working electrode (HMDE), a glassy carbon rod counter electrode, and a double junction Ag/AgCl reference electrode. Potential control and the resulting current readings were obtained using a μAutolab III potentiostat controlled with NOVA software and connected to a VA663 electrode stand (all Metrohm AG). The NOVA software was programmed to repeat the same CSV procedure for many hours reducing the frequency of analysis as the rate of iron ligand exchange reaction decreased.

UV-digestion was carried out using a home-built system consisting of a 150 W high-pressure mercury vapour lamp in 30 mL quartz tubes with a 2-hour irradiation time. The hours period is twice the duration required to cancel the Fe-HS CSV signal obtained with less powerful lamps in coastal and ocean waters (Laglera et al., 2007).

3.2. Reagents and materials

Ultrapure Milli-Q water (Millipore, UK) was used for solution preparation and container rinsing. Iron standards were prepared by dilution in acidified ultrapure water (pH ~1.8) of a 1 ppm atomic absorption spectrometry standard solution (BDH, UK). The iron ligand DHN (2,3-dihydronaphthalene) (Fluka) was prepared in acidified ultrapure water (pH ~1.8) at a concentration of 10 mM. The buffer/catalyst solution was a mixture containing 0.1 M POPSO (piperazine-1,4-bis(2-hydroxypropanesulfonic acid) dehydrate from Sigma Aldrich) and 0.4 M potassium bromate (Sigma Aldrich). The pH of this mixture was raised to 8.2 using ammonia (Ultratrace Fluka). Iron impurities were removed by overnight equilibration with a suspension of MnO_2 followed by filtration (0.2 μm cellulose nitrate, Whatman). A solution of NaCl (ultratrace, Fluka) was prepared at a concentration of 0.72 M to reproduce the ionic strength of oceanic seawater.

Suwannee River fulvic acid (SRFA) and humic acid (SRHA) were

purchased from the International Humic Substances Society (IHSS) and used as model HS. Stock solutions of 0.2 g/L were prepared in Milli-Q water and stored at low temperatures until use. The siderophore desferrrioxamine B (DFOB, (N'-[5-(Acetyl-hydroxy-amino)pentyl]-N-[5-[3-(5-aminopentyl-hydroxy-carbamoyl) propanoylamino] pentyl]-N-hydroxy-butane diamide) was purchased as mesylate salt (Sigma Aldrich) and dissolved in ultrapure water. An aqueous stock solution of DFOB was diluted to a concentration of 5 μM and kept in the fridge between uses. The tetrapyrrole protoporphyrin IX (PP IX, (3,7,12,17-tetramethyl-8,13-divinyl-2,18-porphinedipropionic acid) was chosen as a typical cell lysis ligand. Due to its poor solubility in water and its tendency to dimerize and polymerize as a function of pH (Scolaro et al., 2002), aqueous PP IX solutions require specific pre-planning (see Section 3.3 and the Supplementary Material for details). Stock solutions were prepared by dissolving a few mg in 1 M HCl (ultratrace, Merck), subjected to ultrasound to facilitate solubilisation and brought to 1 L volume. This solution was stored at low temperatures in the dark until use.

A 0.1 M EDTA (Ethylenediaminetetraacetic acid, Merck) solution was prepared in ultrapure water. The pH of the solution was raised to 8.2 with ultratrace grade ammonia.

Reagent solutions and seawater mixtures were prepared in low density polyethylene (LDPE) containers (Nalgene) that had been previously sequentially cleaned with detergent (BIO-SEL), 10 % HCl and 1 M HCl with ultrapure water rinses in between and before use.

The ligand-free seawater used here was a mixture of leftover filtered (0.2 μm) samples from Polarstern cruise ANT-XXV/3 carried out in waters of the Antarctic Ocean (Laglera et al., 2017). The seawater mixture was homogenised in a clean LDPE bottle and UV digested before use to remove any interfering organic matter.

3.3. Analytical limitations of the use of PP IX and EDTA

We found severe analytical drawbacks using PP IX and EDTA with our analytical scheme. With both ligands, we faced the possibility that the sensitivity of the CSV method changed by a small fraction before and after the addition of the competing ligand, preventing an accurate determination of the initial drop in Fe-SRFA concentrations. Although the kinetics obtained were representative of the ongoing reaction, we could under or overestimate the initial concentration drop and therefore concentration of iron exchanged at equilibrium. We consider these experiments mainly for qualitative purposes. We present a detailed description of these drawbacks in the Supplementary Material to warn researchers attempting to reproduce our results.

3.4. Electrochemical parameters

Since the voltammetric behaviour of Fe-HS and Fe-DHN complexes on the HMDE is similar, both methods share the same electrochemical parameters described in previous publications (Laglera et al., 2007; Laglera et al., 2013). Briefly, prior to analysis, oxygen was removed by purging with water-saturated N_2 for 300 s. The iron complexes were deposited on the HMDE by setting the cell potential at −0.1 V for 90 s. After a quiescence period of 7 s, the potential was shifted to −0.7 V using the sampled direct current mode with a scan rate of 50 mV s^{-1}.

3.5. Total dissolved Fe determinations

Iron concentrations in UV seawater or NaCl solution before or after addition of ligands were determined by AdCSV after overnight acidification at pH 2.0 and neutralization with ammonia in the presence of 1,2 dihydroxynaphtalene (DHN) and bromate according to (Laglera et al., 2013). The determination of Fe impurities in the reagents is explained in the Supplementary Material.

3.6. Humic substances binding capacities

The determination of the iron binding capacity of SRFA and SRHA solutions (BC_{SRFA} and BC_{SRFA}) was carried out according to an established procedure (Laglera and van den Berg, 2009). Briefly, 1 mg/L solutions of SRFA or SRHA were titrated in a ligand-free matrix (ultrapure water, 0.72 M NaCL or UV digested seawater) with successive iron additions of a few nanomols L^{-1}. After each iron addition, the solution was purged with N_2 for 5 min to allow the formation of Fe-HS complexes. Three to five CSV analyses were then performed to check the stability of the signal before the next iron addition. The Fe-HS peak increases linearly as a function of the concentration of the added iron until the HS binding groups become saturated. Beyond this stage, the CSV peaks fall below the linear trend and decrease with time due to the slow precipitation of excess iron. The iron concentration corresponding to the intersection of the two related sections was used to determine the iron BC_{SRHS}.

3.7. Iron ligand exchange of Fe-HS complexes

The CSV response of Fe-SRFA complexes was monitored in 20 mL samples (UV seawater or 0.72 M NaCl) spiked with 1 mL of the POPSO/bromate, SRFA or SRHA solution for a cell concentration of 1 mg/L. It is important to underline that the presence of bromate in solution prevents the formation of Fe(II) during the whole procedure. Iron concentration was adjusted to ensure that the sum of dissolved iron in the matrix (0.5 nM for the UV digested seawater and 2.1 nM in 0.7 M NaCl), reagent impurities and the iron spike reached 90–95 % of the BC_{SRHS}. Prior to analysis, the quartz cell was conditioned by filling it three times with the same solution described above and then discarded. Several CSV measurements were taken before introducing the competing ligand to confirm the stability of the Fe-HS signal. After the spike, the first scan was obtained with approximately 100 s delay due to the 90 s deposition period. The Fe-HS concentration was monitored until a steady state concentration was observed for at least 20 min. It is important to note that this setup was neither suitable for resolving kinetics that completed within seconds nor monitor slow reactions (if any) that would require days to complete. The initial Fe-HS concentration, used for calibration, was determined as the CSV signal before the addition of the competing ligand, which equated to the total iron concentration in the cell. For fitting purposes and calculation of kinetic rate constants and conditional stability constant, the decrease in Fe-SRHS complex concentration was quantitatively converted into the concentration of the iron complex formed with the competing ligand ($Fe\text{-}L_{ad}$) and the concentration of dissociated iron-free SRHS (Eq. (1)).

3.8. Reversibility. Sequestering of iron bound to DFOB and PPIX by HS

We studied the reverse case, i.e., the ligand exchange of Fe-FOB or Fe-PPIX complexes in solution after subsequent addition of HS'. We used only SRFA because SRHA, as purchased, is contaminated with iron and, possibly, after dissolution, their stronger binding groups are saturated with iron. In two separate experiments, we spiked UV seawater with 1 mL of the POPSO/bromate solution and 16 nM of DFOB or PPIX and iron at a concentration sufficient to reach a cell concentration of 16 nM iron. As usual, we conditioned the cell with the same solution twice. For analysis, we previously confirmed the absence of interfering electrolabile iron complexes and after 5 min of conditioning we spiked the solution with 2 mg SRFA l^{-1} for a binding capacity of 29.0 nM Fe and monitored the formation of electroactive Fe-SRFA complexes for several hours. At the end of the data collection, we calibrated the Fe-SRFA with three (DFOB) or four (PPIX) internal additions of 2 nM Fe to determine the sensitivity.

3.9. Studies of the formation of HS and DFOB adducts

We investigated whether HS and DFOB interact, leading to the formation of HS-DFO and/or HS-Fe-FOB adducts using our voltammetric method. Despite the limitations of non-spectroscopic methods, electrochemical methods offer the advantage of conducting experiments under conditions close to natural concentrations. The iron concentration was kept well in excess of the combined binding capacities of FOB and HS to avoid any net iron ligand exchange. However, organic-organic interactions may introduce deviations from the expected stable CSV signal caused by iron-saturated HS. We conducted a preliminary experiment with immediate monitoring of reagent in-cell additions, which unfortunately was affected by iron precipitation. The interpretation of the results from this experiment was not straightforward, and a detailed account can be found in the Supplementary Material. This information is provided to prevent other researchers from attempting to use a similar analytical scheme without considering the potential challenges related to iron precipitation.

We prepared two sets of 30 mL LDPE bottles containing 10 mL aliquots of UV-digested seawater. We then sequentially spiked HS (first set with 2 mg/L SRFA and the second set with 1 mg/L SRHA, for BC_{SRHS} of 29.0 and 32.1 nM Fe, respectively), DFOB (range 0 to 100 for SRFA and 0 to 300 for SRHA with sufficient time to interact) and, finally, 600 nM Fe to saturate all ligands. We allowed the mixture to interact overnight to allow precipitation of excess iron and the next day all aliquots were spiked with bromate/POPSO reagent and analysed by CSV to check whether siderophore-HS interactions could have prevented the equal formation of electrolabile Fe-HS complexes.

3.10. Modelling of kinetics of iron ligand exchange mechanisms

The Dynafit numerical resolution program (Kuzmič, 1996) was used for the global fitting of the experimental data. This program utilizes the Levenberg-Marquardt algorithm to perform least-squares fittings of the kinetic tracer time course. Three iron ligand exchange mechanisms were tested to explore the reaction mechanisms before the accumulation of experimental evidence led us to propose a refined mechanism: i) homogeneous reversible iron ligand exchange, ii) reversible heterogeneous iron ligand exchange with two types of departing complexes, Fe-$SRHA_1$ and Fe-$SRHA_2$, and iii) irreversible heterogeneous iron ligand exchange, where we assume the existence of a ternary intermediate in equilibrium with the departing species, but with slow dissociation kinetics (detailed in Section 4.10).

The mechanism equations, definition of the kinetic rate constants and the number of species fitted for each of the three mechanisms can be found in the Supplementary Material. Access to Dynafit scripts and experimental data is detailed in the Data availability statement.

4. Results and discussion

4.1. Binding capacities of different IHSS reference materials in various matrices

Our experimental design required the saturation of the departing ligand and absence of excess inorganic iron in the cell. Therefore, accurate determination of the iron contamination of the reagents and the BC of the IHSS reference FA or HA was essential. Table S1 shows the BC_{SRHS} of different IHSS standards (purchased and analysed through the years) dissolved in UV-digested seawater, ultrapure water, and NaCl 0.72 M.

Despite the two decades between the first Suwannee River extraction (1R101) and the one currently available from IHSS (1S101), both the iron BC_{SRFA} and BC_{SRHA} have remained constant. This is convenient for the type of study presented here, as it allows comparison of values found in the literature regardless of the batch used in the experiments. The iron BC_{HS} in ultrapure water were much higher than in seawater, indicating a competition of cations for iron binding moieties. Removal of divalent cations (0.72 M NaCl) did not lead to an increase in the BC found in seawater. This indicates that the reduction in iron binding due to the increase of the ionic strength is not due to specific competition with divalent cations.

4.2. Iron ligand exchange of iron-saturated Fe-SRFA complexes after addition of DFOB

The addition of iron-free DFOB to seawater containing iron-saturated SRFA gave the predicted decrease over time of the CSV signal of the Fe-SRFA complexes (Fig. 1). In all three experiments, the initial concentration of SRFA was 1 mg SRFA L^{-1} (binding capacity of 14.5 ± 0.7 nM Fe) to which Fe was added to have an in-cell concentration of 14.1 nM Fe, approximately 97 % saturation of the SRFA binding sites. After addition of 15, 30 and 50 nM DFOB (equivalent to 1 to 3.5 times the BC_{SRFA}), we observed an immediate sharp decrease in the Fe-SRFA signal followed by slower kinetics until a stable concentration of Fe-SRFA remained in solution (Fig. 1). This type of result indicates a reversible reaction in which the concentrations of both complexes reach a dynamic equilibrium (Eq. (1)). The ratio between the iron complexes is controlled by the remaining concentration of iron-free ligands and the ratio of their conditional stability constants (Eq. S5).

Firstly, we will focus on the pre-equilibrium kinetics. In the first ~ 100 s required to complete the first measurement after the addition of DFOB, the initial Fe-SRFA signal plummeted as a function of the added DFOB concentration by 18, 22 and 33 %, respectively (red arrows in Fig. 1). This immediate exchange of about one third of the iron bound to SRFA could be interpreted as weakly bound iron (binding groups characterized by low $K'_{Fe'\text{-}SRFA}$ and high dissociation kinetics), according to a D mechanism. Thereafter, a period of 0.5 to 3 h of slow exchange kinetics started, whereby the higher the DFOB concentration added, the sooner equilibrium was reached. However, this behaviour contradicts what is expected according to a D mechanism, where the period before equilibrium depends mainly on the dissociation kinetics of the initial complex and hardly on the nature or concentration of the incoming ligand (Fig. S4).

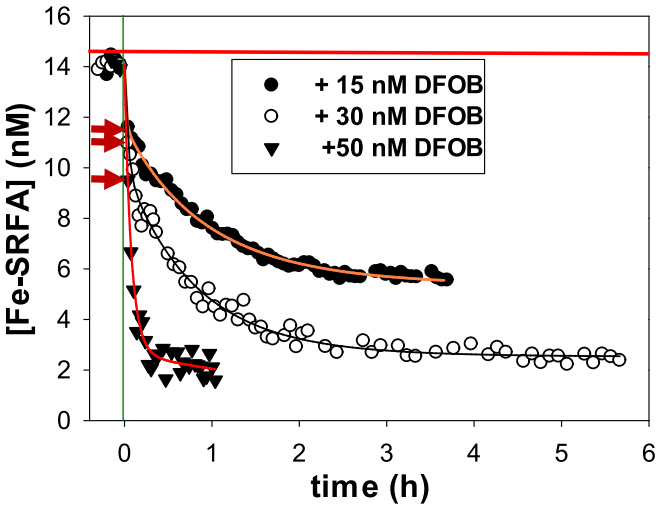

Fig. 1. Time course of the concentration of Fe-SRFA complexes in UV-digested seawater in response to different additions of iron-free DFOB. Prior to DFOB addition, SRFA solutions (1 mg/L, BC_{SRFA} of 14.5 ± 0.7 nM Fe) were spiked with iron to nearly saturate the binding sites. Solid red lines mark the BC_{SRFA}. The red arrows on the left indicate the first measured concentration, approximately 2 min after DFOB addition. The lines are the result of fitting the concentration kinetics to the reaction model shown in Section 4.10. (For interpretation of the references to colour in this figure legend, the reader is referred to the web version of this article.)

Secondly, we will focus on the species partitioning at equilibrium. We found that DFOB additions of 1 to 3.5 times the BC_{SRFA} left 39, 18 and 15 % of the initial Fe-SRFA signal at equilibrium, respectively (Fig. 1). Use of Eq. S5 gave $K'_{Fe'\text{-}DFOB}/K'_{Fe'\text{-}SRFA}$ ratios of 2.0, 3.1 and 2.0 at increasing DFOB concentrations, respectively (average 2.4). Although this result is consistent with a weaker affinity for iron of the SRFA binding groups, the $K'_{Fe'\text{-}DFOB}$ value was only slightly higher than that of $K'_{Fe'\text{-}SRFA}$.

In the case of the interaction of iron and HS, the common paradigm in aquatic chemistry is that all HS binding sites are weak and can hardly compete against natural ligands of biological origin and higher affinity for iron (Whitby et al., 2020b). The origin of such a belief is the initial estimation by CLE-AdCSV of log $K'_{Fe'\text{-}SRFA}$ at 10.6, using dihydroxynaphtalene as L_{ad}, which was at least one logarithmic unit lower than log $K'_{Fe'\text{-}DFOB}$ determined at values between 11.6 using 1-nitroso-2-naphtol as L_{ad} and > 13 using salycilaldoxime and 2-(2-thiazolylazo)-p-cresol as L_{ad} (Croot and Johansson, 2000; Laglera and van den Berg, 2009; Rue and Bruland, 1995; Witter et al., 2000). Our low $K'_{Fe'\text{-}DFOB}/K'_{Fe'\text{-}SRFA}$ ratio is not unique in the sense that it concurs with two previous works in which the addition of DFOB in large excess of iron to HS-rich samples could only extract a fraction of the HS-bound iron (Kuhn et al., 2014; Laglera et al., 2019).

4.3. Iron ligand exchange of iron-partially saturated Fe-SRFA complexes after addition of DFOB

The experiment detailed above was repeated by reducing the concentration of added iron by approximately 3 nM (for 11 nM Fe in cell) (Fig. 2). This roughly corresponds to the concentration of binding groups that interchanged iron with DFOB in less than 100 s in the experiment shown in Fig. 1. The aim was to better characterize the SRFA iron binding groups that experienced slow interchange kinetics in the previous experiment. According to a D mechanism, iron at a concentration below the BC_{SRFA} would be preferentially bound to slower-dissociating and higher stability ligands. Thus, by reducing the concentration of iron in solution, the fast dissociating SRFA binding groups would be left free of iron and, therefore, the iron ligand exchange kinetics would show only the exponential decreasing section without the initial fast drop of ~20 % (red arrows in Fig. 1).

However, this was not the observed behaviour (Fig. 2). The addition of 10 and 15 nM DFOB also resulted in a rapid drop of the CSV signal in the first 100 s, in this case 3.2 and 5 nM Fe-SRFA complexes, respectively. This is approximately the same initial Fe-SRFA concentration drop observed at higher iron concentrations (red symbols in Fig. 2). Therefore, the rapid initial iron ligand exchange observed in Fig. 1 does not appear to be caused by a very low stability of one third of the SRFA binding groups.

In this case, the iron ligand exchange reached equilibrium in ~1 h, which is approximately three times faster than observed after near full saturation of the SRFA. HS iron saturation appears to be geochemically relevant since this exchange period is substantially shorter than the periods required to complete other relevant biogeochemical processes (refer to Section 4.2). The concentration of Fe-SRFA complexes that remained at equilibrium were of 3.9 and 2.5 nM, respectively, lower with respect to the experiments under near saturation (open symbols in Fig. 2) but in concurrence the lower iron availability. The decrease in Fe-SRFA concentration was similar to the decrease observed under saturation of the binding groups (black and red double headed arrows in Fig. 2, respectively). This same ability to extract iron despite the presence of more iron-free SRFA binding groups translates into $K'_{Fe'\text{-}DFOB}$ / $K'_{Fe'\text{-}SRFA}$ ratios of 8.1 and 7.4, about three times higher than the values found under near SRFA saturation. Proper interpretation of this result against the common understanding of complexation is discussed in section 4.9.

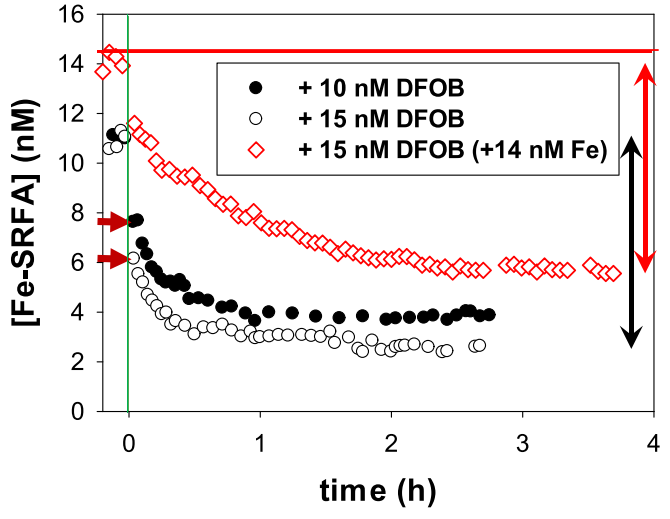

Fig. 2. Time course of the concentration of Fe-SRFA complexes (1 mg SRFA L^{-1}) after addition of 10, and 15 nM DFOB. The red line represents the BC_{SRFA}. The red thick arrows indicate the first concentration obtained approximately 100 s after addition of DFOB. The double headed arrows indicate the magnitude of the decrease in Fe-SRFA at equimolar DFOB additions. The red diamonds correspond to the addition of 15 nM DFOB in Fig. 1 shown for comparison. (For interpretation of the references to colour in this figure legend, the reader is referred to the web version of this article.)

4.4. Labilization effect of seawater major bivalent cations

Seawater cations can interfere with ligand exchange reactions by increasing the lability of the complexes and thus their dissociation (Boiteau and Repeta, 2022; Laglera and Filella, 2015). The major bivalent cations, Mg^{2+} and specially Ca^{2+}, are expected to have a great impact (Fujii et al., 2008; Hering and Morel, 1988; Schijf and Burns, 2016). Mechanistically, this interaction can be caused by occupation of the iron binding sites (of one or more binding groups in multidentate complexes) or by forcing changes in the spatial arrangement of the complex (Wilkins, 1991).

We repeated the iron ligand exchange kinetic experiment after the addition of 30 nM DFOB to 1 mg SRFA L^{-1} nearly saturated with iron using now a 0.72 M NaCl matrix to maintain the ionic strength of

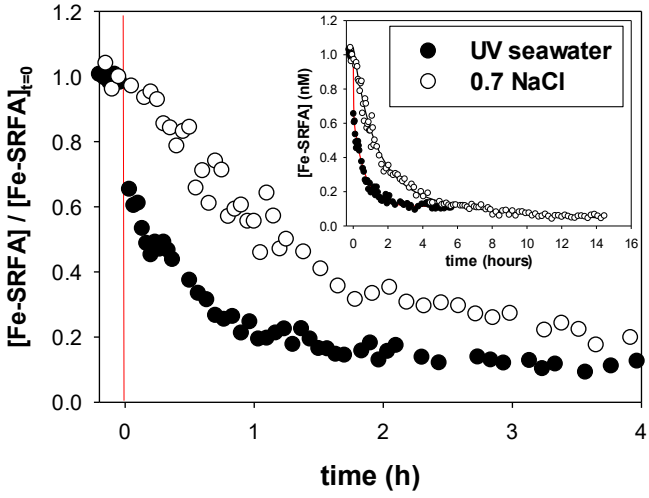

Fig. 3. Effect of divalent cations on the kinetics of iron ligand exchange: time course for the first 4 h (to highlight the lack of fast initial signal drop) of the concentration of Fe-SRFA complexes after addition of 30 nM DFOB to 1 mg SRFA L-1 saturated at 90 % in UV seawater and in 0.72 M NaCl. Insert plot: the complete experiment.

seawater while eliminating any effect of bivalent cations (Fig. 3). The kinetic section showed two differential features compared to the seawater experiments. First, the immediate drop of the Fe-SRFA signal was absent here (Fig. 3). Thus, matrix effects and not an extremely low affinity of a fraction of the SRFA binding groups for iron controlled the initial fast dissociation of Fe-SRFA complexes in UV seawater shown in Figs. 1 and 2. Second, the time needed to reach equilibrium was much longer, approximately 12 h, implying that Ca^{2+} and Mg^{2+} in solution act as accelerators of iron ligand exchange of Fe-HS complexes in seawater. In estuaries, as salinity increases, the cancellation of DOM (and HS) negative charges flocculation and precipitation. From our results, we can infer that this is parallel to an acceleration of ligand exchange reactions, which may help to reduce the percentage of precipitated iron by exchanging it with more soluble organics. Our results are in agreement with a previous study that found that additions of Ca^{2+} or Mg^{2+} ions at concentrations similar to those found in seawater substantially retarded the exchange of iron ligands from FA complexes to 5-sulfosalicylic acid in NaCl solutions (Fujii et al., 2008). Apart from bond perturbation by divalent cations, other phenomena characteristic of HS, such as SRFA conformational changes and alteration of molecule bridging, might have played a role.

At equilibrium, DFOB had sequestered more iron, with only 0.7 nM Fe-SRFA remaining in solution (about 5 % of the binding capacity) (Fig. 3). Thus, the removal of bivalent cations increased the competing ability of DFOB. As a result, the $K'_{Fe'\text{-FOB}}$ /$K'_{Fe'\text{-SRFA}}$ ratio was of 13.9, an increase by a factor of ~5 with respect to seawater that could be caused by possible conformational changes and/or by a higher affinity of Ca^{2+} and Mg^{2+} for the iron binding sites of the SRFA than for those of DFOB. The lack of related literature prevents us from confirming or rejecting each hypothesis.

4.5. Iron ligand exchange of iron saturated Fe-SRHA complexes after addition of DFOB

HA are characterized by higher hydrophobicity, higher average molecular weight, and BC_{SRHA} nearly twice as large than FA extracted from the same source (Table S1). Unfortunately, there is no information in the literature on the kinetics of iron ligand exchange of Fe-SRHA complexes. Previous estimates by CLE-AdCSV using dihydroxynaphtalene, salycilaldoxime and EDTA as L_{ad} have shown that the average stability of Fe-SRHA complexes is slightly higher than that of SRFA with log $K'_{Fe'\text{-SRHA}}$ in the range 11.1–11.6, about half a logarithmic unit higher than log $K'_{Fe'\text{-SRFA}}$ (Abualhaija and van den Berg, 2014; Laglera and van den Berg, 2009). However, in a recent intercalibration exercise, SRFA was found to be stronger or weaker than SRHA depending on L_{ad} (Gerringa et al., 2021). This discrepancy is possibly due to methodological artefacts caused by the hydrophobicity of HS; which is more pronounced in the HA fraction.

We observed the same plummeting of the Fe-SRHA signals that increased from 10 to 16 nM Fe when the concentration of DFOB increased from equimolar to 7.5 times the iron BC_{SRHA} (Fig. 4). At equilibrium, the Fe-SRHA concentrations were in the range of 52 to 16 % of the initial concentration, substantially higher than those found for Fe-SRFA. The $K'_{Fe'\text{-DFOB}}$ / $K'_{Fe'\text{-SRHA}}$ ratios obtained with increasing DFOB additions equal to or higher than the BC_{SRHA} were in a narrow range, 0.73, 0.38, 0.38, 0.74 and 0.69 in order of increasing DFOB concentrations (Fig. 4). Therefore, $K'_{Fe'\text{-SRHA}}$ was consistently higher than $K'_{Fe'\text{-DFOB}}$. Geochemically, this finding represents a shift in the paradigm that all HS binding groups are weak binding groups and will require a redefinition of the role of HS in ocean iron cycling and of the constituents of the ligand classifications published to date (Buck et al., 2015).

We added in one experiment only 10 nM DFOB to nearly iron-saturated SRHA (Fig. 4). Since the addition of 35 nM DFOB decreased the Fe-SRFA signal in the first 100 s of the experiment by 6.2 nM Fe, according to a D mechanism, we expected a fast decrease of similar magnitude due to the favoured dissociation of weak binding groups.

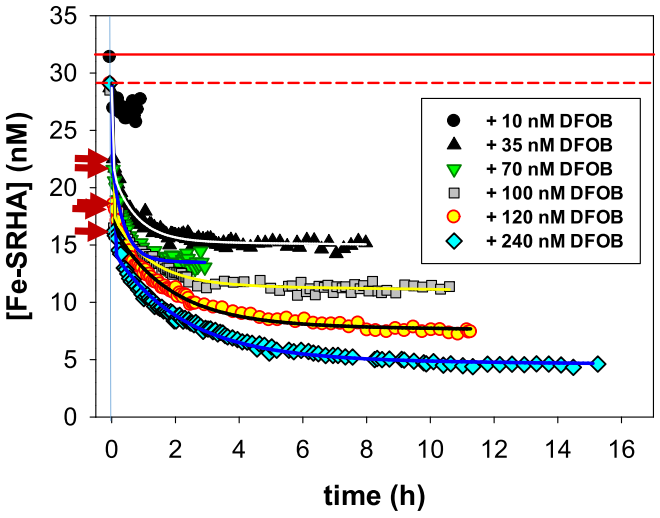

Fig. 4. Time course of the concentration of Fe-SRHA complexes when SRHA at a concentration of 1 mg/L dissolved in UV-digested seawater and saturated to 90 % of its iron binding capacity is spiked with different concentrations of DFOB. The solid red line marks the BC_{SRHA}. The dashed red line marks the initial concentration of Fe-SRHA complexes (except for the addition of 10 nM DFOB, see text for details). The lines are the result of fitting the concentration kinetics to the reaction model shown in Section 4.10. (For interpretation of the references to colour in this figure legend, the reader is referred to the web version of this article.)

However, the addition of 10 nM DFOB reduced the Fe-SRFA signal by only 4.5 nM Fe-SRFA in the initial 100 s and barely more in the following 55 min (4.7 nM Fe at the end of the experiment). Thus, approximately 5 nM of DFOB remained iron free at the equilibrium despite the presence of approximately 26 nM of Fe-SRHA complexes. The limited ligand exchange resulted in a $K'_{Fe'\text{-DFOB}}$ / $K'_{Fe'\text{-SRFA}}$ ratio 0.19, indicating strong complexation by SRHA despite our expectation that only loosely bound iron would be involved.

The experiments with higher DFOB additions showed a period of slow kinetics after the initial rapid decrease of the Fe-SRHA signal that lasted approximately 2 to 11 h until equilibrium was reached (Fig. 4). Contrary to our findings for SRFA, this period before reaching equilibrium was longer with higher additions of DFOB. The behaviour could be caused by the higher heterogeneity and overall affinity for iron of SRHA. As the DFOB concentration increases, it mobilizes iron from the HS binding groups with higher affinity for iron and slower dissociation kinetics resulting in a longer time to reach equilibrium. However, this would not coincide with our observation after addition of 10 nM DFOB.

From a geochemical standpoint, it is important to underline that the kinetic period of ligand exchange of Fe-SRHS complexes in seawater is comparable to the periods described for completing iron cell uptake and aggregation to colloids, taking many hours (Fox and Wofsky, 1983; Shaked et al., 2020), and faster that the period of a few days described for iron precipitation (Liu and Millero, 1999, 2002). In the ocean, reactions with similar kinetic rates would progress at a similar rate, substantially complicating the prediction of iron speciation, partitioning and cycling.

4.6. Iron ligand exchange of iron saturated Fe-SRHS complexes after addition of other ligands

Since a D mechanism produces similar ligand exchange kinetics regardless of the nature of the competing ligand (Helm and Merbach, 2005; Wilkins, 1991), we repeated our experiments using two other commonly used ligands in CLE experiments. Specifically, the pigment precursor PP IX, which has shown conditional stability constant and formation and dissociation kinetics similar to those of DFOB in previous

CLE-AdCSV studies (Witter et al., 2000), and EDTA. With both ligands, although the kinetics obtained were representative of the ongoing reaction, we faced the possibility that the sensitivity of the method changed by a small fraction immediately after addition of the competing ligand. This drawback and its consequences are detailed in the Supplementary Material of this manuscript.

Fig. 5 A shows the kinetics of iron ligand exchange after addition of 1.3 mM EDTA to UV seawater spiked with 2 mg SRFA L^{-1} and 1 mg SRHA L^{-1}, respectively. Fig. 5 B shows the same experiment with additions of 15 and 30 nM PP IX to 1 mg SRFA L^{-1}. With both ligands, we observed the same rapid initial decrease of the Fe-HS signal, as seen with DFOB in seawater (red arrows in Fig. 5). Thus, the immediate loss of a substantial fraction of Fe-SRFA complexes upon interaction with divalent cations in seawater occurs regardless of the nature of the competing ligand. However, there was an important difference with the results shown in Fig. 1: the period required to reach equilibrium with EDTA was of 18 to 20 h, 2 to 6 times the time required for DFOB while for the addition of 15 nM and 30 nM PP IX it was less than 1 h and about 3 h, respectively, shorter than for DFOB (see Fig. 1). This is indicative that the iron ligand exchange of Fe-SRHS complexes follows an A route.

Equilibrium iron partitioning also provides valuable information. In the case of EDTA, there are published stability constants with all major cations in seawater. These constants enable that from $K_{Fe'\text{-}EDTA}$, it is possible to estimate that the log $K'_{Fe'\text{-}EDTA}$ in a seawater matrix is 7.97 (Croot and Johansson, 2000; Laglera et al., 2011). From the use in Eq 4 of the mass balances of iron, HS and EDTA (Eq. S3) along with log $K'_{Fe'EDTA}$ of 7.97, and log $K'_{Fe'SRFA} = 10.6$ or log $K'_{Fe'SRHA} = 11.1$ (Laglera and van den Berg, 2009), it can be estimated that only 1 and 3 % of the Fe-SRFA and Fe-SRHA complexes, respectively, should have remained in solution at equilibrium. The data presented in Fig. 5A corroborate the prior underestimation of $K'_{Fe'SRHA}$ and $K'_{Fe'SRHA}$. Apparent equilibrium was reached when approximately 30 % (2 mg SRFA L^{-1}) or 40 % (1 mg SRHA L^{-1}) of the initial Fe-SRHS concentration remained in solution.

A similar result was obtained with PP IX. In a previous CLE-AdCSV experiment the log $K'_{Fe'PPIX}$ was found to be 0.8 logarithmic units higher than log $K'_{Fe'DFOB}$ (Witter et al., 2000). The same calculations shown above using Eq. S3 and S5, indicate that after adding 15 and 30 nM PP IX, respectively, the concentration of Fe-SRFA complexes in seawater should have decreased to 8.7 and 1.4 % of the initial concentration. However, Fig. 5B shows again that the concentration of Fe-SRFA binding groups remaining in solution was much higher, at 57 and 32 %, respectively. The $K'_{Fe'PP\ IX}/K'_{Fe'SRFA}$ ratios were found to be 0.6 and 1.1 for 15 and 30 nM PP IX, respectively, indicative that in seawater, SRFA and PP IX have similar affinities for iron.

Even when accounting for the uncertainty brought by small pH changes after the introduction of the competing ligand, both experiments again confirm that the stability of Fe-SRHS complexes is substantially higher than previously reported in the literature.

4.7. Heterogeneity of the SRHS binding sites

While other CLE and spectroscopic methods have been successful in distinguishing between weak and strong SRFA binding groups (Heerah and Reader, 2022; Rose and Waite, 2003), SRFA binding heterogeneity for iron has proven elusive to CLE-AdCSV despite various attempts using different competing ligands (Gerringa et al., 2021; Laglera et al., 2011; Laglera et al., 2020). This was not the case for SRFA and copper which showed clear binding heterogeneity (Kogut and Voelker, 2001; Muller and Batchelli, 2013).

Although strongly influenced by the mobilizing effect of the main bivalent cations, the binding heterogeneity during iron ligand exchange of Fe-SRHS complexes is indicated by the presence of two distinct kinetic periods. The presence of more than one type of binding groups curves the otherwise linear characteristic plot of second order kinetics (Fig. S2) and this curvature is observed in all experiments shown in Figs. 1 to 4 with the exception of the addition of 50 nM DFOB to SRFA and the experiment in 0.7 M NaCl (Fig. S5).

In Fig. 6, we show two examples of iron ligand exchange and the characteristic plots of second order kinetics. One example involves SRFA complexes, while the other pertains to SRHA complexes. The 1/[Fe-SRHS] vs. time plots from the rest of experiments can be found in Figs. S6 and S7. Deviations from linearity were not limited to the first two points, thus the heterogeneity extends beyond the initial concentration drop. Fig. 6 also shows the substantial improvement resulting from modelling the addition of a second type of SRHS binding groups with different exchange kinetics to the reaction mechanism. In the case of SRFA, there were two pseudolinear segments with different slopes, one for the first 15–20 min and a second for the remainder before equilibrium. In the case of SRHA, the curvature is more pronounced and more sections are apparent upon visual inspection (Fig. 6D). We believe that this is due to the presence of more types of binding groups and that reaction models with more types of binding groups could give better fits. We plan to explore the possibilities of this line of work in the future.

Iron binding by DOM has often been described as a combination of "specific" (chelation) and "non-specific" (long range electrostatic attraction) interactions, with the latter being necessarily more susceptible to competition (Morel and Hering, 1993). Other authors refer to these two classes as chelated (mostly bidentate) and bridging iron

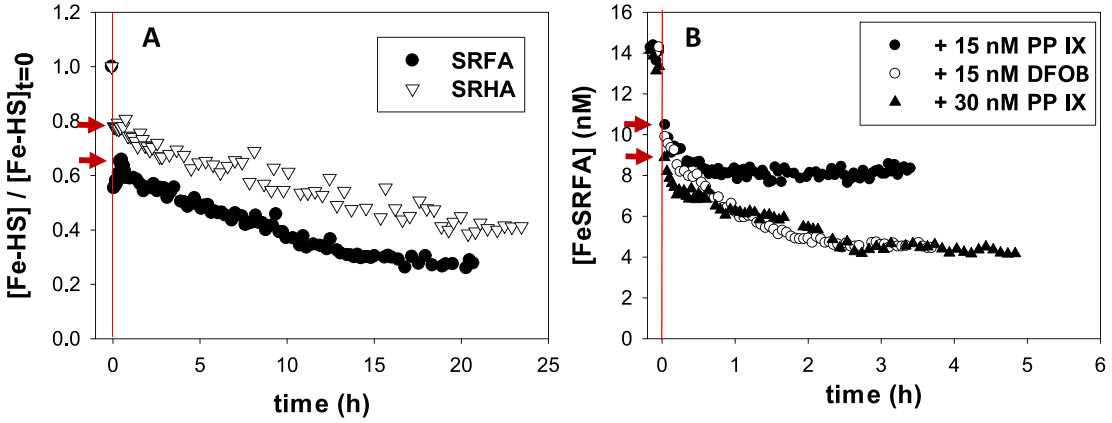

Fig. 5. (A) Time course of the normalized concentration of Fe-SRFA and Fe-SRHA complexes in UV-digested seawater in response to the addition of 1.3 mM EDTA. The initial concentrations were 2 mg SRFA L^{-1} and 1 mg SRHA L^{-1}, respectively (equivalent to iron BC of 29 nM and 32.6 nM Fe, respectively). (B) Same experiment with the addition of 15 and 30 nM PPIX; it was checked that at the end of the experiment the pH drop was less than 0.1 pH units. All solutions were spiked with iron in order to almost saturate (90 %) their binding sites. The red arrows indicate the first concentration obtained approximately 100 s after the addition of the competing ligand. (For interpretation of the references to colour in this figure legend, the reader is referred to the web version of this article.)

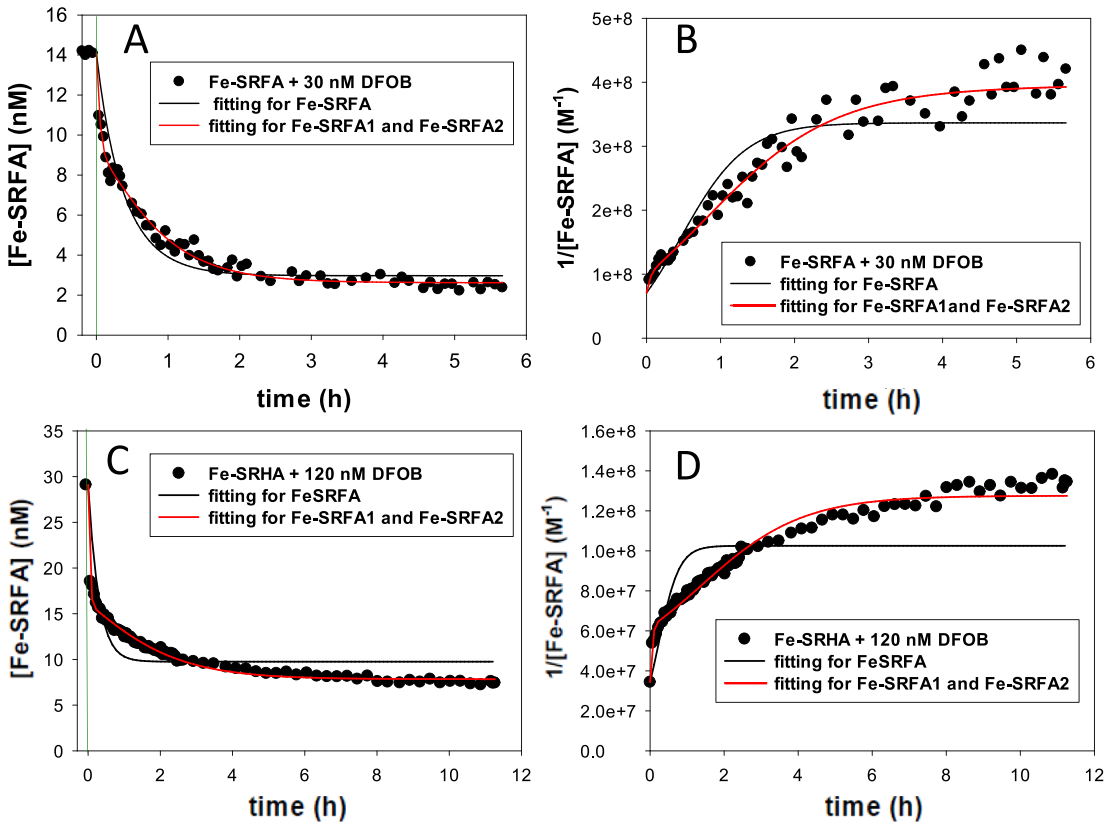

Fig. 6. A and B: A is the experimental results of the addition of 30 nM DFOB to 1 mg SRFA L^{-1} and B is the characteristic plot of second-order kinetics. The lines are non– linear fittings of Eq. (1) (black) and Eq. (1) modified to include two types of binding sites (red). C and D: the same for the addition of 120 nM DFOB to 1 mg SRHA L^{-1}. A: the kinetic rate constants obtained according to an heterogeneous mechanism were $k_2 = 1.58 \pm 0.25$ and $k_{-2} = 0.574 \pm 0.019$ x10^4 $M^{-1}s^{-1}$ for the forward and backward ligand exchange of Fe-$SRFA_1$ complexes and $k_1 = 4.28 \pm 0.36$ and $k_2 = 59.4 \pm 5.8$ x10^4 $M^{-1}s^{-1}$ for Fe-$SRFA_2$ complexes. B: for the same model, $k_3 = 0.161 \pm 0.003$ and $k_4 = 0.278 \pm 0.007$ x10^4 $M^{-1}s^{-1}$ for the forward and backward ligand exchange of Fe-$SRHA_1$ complexes and $k_1 = 1.88 \pm 0.09$ and $k_2 = 21.2 \pm 1.1$ x10^4 $M^{-1}s^{-1}$ for Fe-$SRHA_2$ complexes (see Supplementary Material for details). (For interpretation of the references to colour in this figure legend, the reader is referred to the web version of this article.)

(Boguta et al., 2019). It is likely that our loosely bound iron is related to the non-chelated fractions referred to in the literature with Ca^{2+} and /or Mg^{2+} disrupting the electrostatic attraction and thereby modulating the initial interaction of SRFA-bound iron and DFOB.

4.8. Iron ligand exchange of Fe-DFOB and Fe-PP IX complexes in the presence of HS. Reversibility

We have defined Eq. (1) as reversible and this seems to be in agreement with the decrease of the initial complex to a steady state observed in all experiments (Figs. 1 to 5). To confirm such reversibility, we repeated our experimental scheme twice using 16.4 nM Fe-FOB and 16 nM Fe-PP IX as the initial complex and SRFA' as the sequestering ligand. Iron was carefully added for a concentration of 16 nM (including reagent contamination) to fix the concentration of the complex to almost 100 % the ligand saturation. The initial ligand saturation prevented the presence of both, significant concentrations of free dissolved iron that could bind to free SRFA and reduce iron ligand exchange or free ligand that could sequester iron impurities form the SRFA reagent. Measurements of reagent impurities gave a concentration of 0.95 nmol Fe mg $SRFA^{-1}$ (batch 1R101F, the one with the lowest contamination, Table S1) implying that approximately 6 % of the SRFA binding groups (presumably those with the higher affinity for iron) were not involved in the ligand exchange reaction. In both cases, after cell equilibration, we added 2 mg SRFA L^{-1}, containing 31.45 nM of iron-free SRFA iron binding groups, for a total in-cell iron concentration of 17.9 nM and monitored the formation of Fe-SRFA complexes (Fig. 7).

For a fully reversible system, with our average $K'_{Fe'\text{-}DFOB}/K'_{Fe'\text{-}SRFA}$ ratio of 2.37, using Eqs. 2 and 4, the theoretical partitioning of species at the equilibrium was estimated to be 45 % of Fe-DFOB and 55 % of Fe-SRFA complexes. For PP IX, the estimate was 34 % as Fe-PP IX and 66 % as Fe-SRFA complexes (using our $K'_{Fe'\text{-}DFOB}/K'_{Fe'\text{-}PPIX}$ ratio of 1.1).

For Fe-PPIX complexes, the formation of Fe-SRFA complexes occurred rapidly within the first 30 min (dissociation of approximately one third of the initial Fe-PPIX concentration), followed by a slower kinetic phase that extended for over 4 h before reaching an apparent equilibrium (Fig. 7). This trend confirmed the reversibility of the reaction and the two step kinetics observed for the forward ligand exchange kinetics (Fig. 5B). The first value (2.3 nM Fe-SRFA) is a composite of the SRFA contamination (1.9 nM Fe) and the concentration of Fe could be sequestered by the SRFA in the first ~ 100 s. By the time we stopped the experiment, the Fe-SRFA concentration had apparently stabilized at 10.4 nM Fe-SRFA, equal to 58 % of the total in-cell iron concentration, which is close to the predicted value of 55 %. However, the kinetics of ligand exchange were substantially slower than predicted by assuming reversibility of ligand exchange between SRFA and PP IX (Fig. 5B). The kinetic rate constants for the addition of 30 nM PP IX to 1 mg/L of SRFA (Fig. 5B) were $k_3 = 0.679 \pm 0.020$ and $k_4 = 0.678 \pm 0.042$ x10^4 $M^{-1}s^{-1}$ for the dissociation and formation of Fe-$SRHA_1$ complexes and $k_1 = 13.9 \pm 0.78$ and $k_2 = 80.3 \pm 5.0$ x 10^4 $M^{-1}s^{-1}$ for Fe-$SRHA_2$ complexes. Since we do not know the contribution of $SRFA_1$ and $SRFA_2$ to Fe-SRFA, we modelled in Fig. 6 the formation of Fe-SRFA twice. Firstly, we assumed that all SRFA binding sites were fast dissociation sites and secondly, we assumed that all of them were slow dissociation sites. In both cases, the dissociation of Fe-PP IX complexes or the formation of Fe-SRFA complexes is clearly slower, indicating that the nature of the incoming ligand

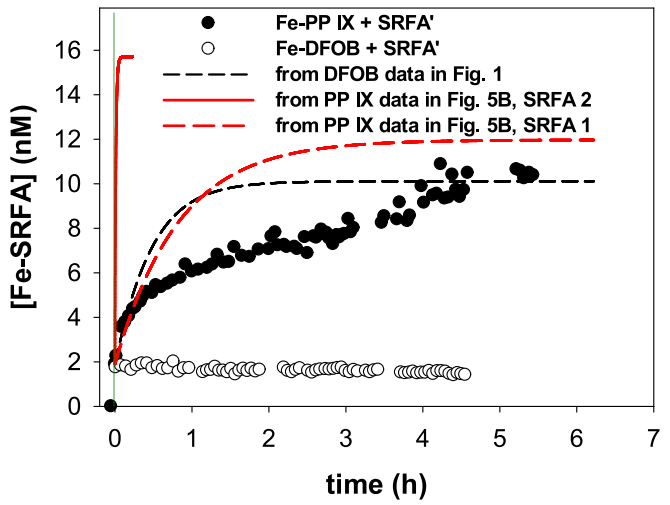

Fig. 7. Time course of Fe-SRFA complex formation when 2 mg SRFA L-1 are added to two aliquots of UV seawater previously spiked with 16 nM of PP IX and DFOB, respectively. The maximum value on the Y-axis is equal to the total concentration of iron in the cell (17.9 nM). The black solid line is the result of calculating Fe-SRFA formation from the kinetic rate constants obtained according to Eq. (1) for the addition to 1 mg SRFA L^{-1} of 30 nM DFOB (Fig. 1, k1 = 0.0727 $M^{-1}s^{-1}$ and k_{-1} = 0.0317 $M^{-1}s^{-1}$). Red lines are the result of using data fitted for the addition of 30 nM PP IX to 1 mg SRFA L^{-1} (Fig. 4). The solid line models Fe-SRFA concentrations calculated assuming that all the SRFA binding sites are fast dissociation sites. The dashed line models Fe-SRFA concentrations calculated assuming that all the SRFA binding sites are slow dissociation sites. See Section 4.8 for details. (For interpretation of the references to colour in this figure legend, the reader is referred to the web version of this article.)

dictates the kinetics of ligand exchange and thus points to an A mechanism.

In the other experiment, these identical SRFA iron binding sites were unable to sequester any iron that had been previously complexed with DFOB. We even observed a small slow signal decrease, equivalent to nearly 1 nM Fe-SRFA. We interpret this trend as the slow removal of the 1.9 nM Fe present as an impurity in the SRFA by the small initial concentration of iron-free DFOB (about 0.4 nM). Fe-DFOB complexation in seawater is thus irreversible upon competition with SRFA.

The partial dissociation of the Fe-DFOB complexes within few hours after addition of small-sized L_{ad} was confirmed in several prior publications (Croot and Johansson, 2000; Witter et al., 2000). The striking difference shown here must be related to the tridimensional conformation of both iron complexes at pH 8 and the size of HS (Gledhill, 2001; Witter et al., 2000). The four nitrogen bases of the tetrapyrrole core of PP IX that bind iron form a square plane. This spatial arrangement allows interactions of solvent molecules and matrix components located perpendicular to the plane. Ligands and accelerators can interact with the iron atom even before dissociation of any of the aforementioned bonds, thus labilizing the Fe-N bonds. On the other hand, the spatial conformation of the Fe-DFOB complex at pH 8.2 is hexadentate with the oxygen and nitrogen bases of three hydroxamate groups completely surrounding the iron ion free of coordinated water molecules. This implies that there is no physical space left to allow direct interaction of matrix components that could labilize the Fe-DFOB bonds, at least above a certain size. In our context, the molecular sizes of the HS are substantially larger compared to the average size of the electrolabile ligands used in CLE-AdCSV and in particular, for the case presented here, the siderophores. It is evident that size hinders the physical approach of HS to a distance that could provoke the destabilization of one of the Fe-DFOB complex bonds.

4.9. Mechanism of iron ligand exchange of Fe-HS complexes with DFOB

According to the evidence we have gathered in this study, the intimate mechanism of iron ligand exchange from SRHS complexes to DFOB in seawater must take into account the following facts:

- the reaction pathway is A because the kinetics of iron ligand exchange is a function of the nature of the competing ligand.
- Iron binding SRHS cannot be described by a single type of binding group. Although this is strongly modulated by matrix effects (which we do not include in our mechanism), it is necessary to define (at least) two different groups of binding sites according to their exchange kinetics ($SRFA_1$ and $SRFA_2$). The difference here with respect to the traditional L_1/L_2 ligand classification is that we adopt a kinetic rather than an affinity criterion.
- the overall reaction is irreversible.

The following reaction mechanism fulfils all three premises:

$$Fe-SRFA_1 + DFOB \overset{k1,-k2}{\longleftrightarrow} Fe-SRFA_1-DFOB \overset{k5}{\longrightarrow} Fe-FOB + SRFA1 \quad (2)$$

$$Fe-SRFA_2 + DFOB \overset{k3,-k4}{\longleftrightarrow} Fe-SRFA_2-DFOB \overset{k6}{\longrightarrow} Fe-FOB + SRFA2 \quad (3)$$

where k_1 and k_3 are the kinetic rate constant of the association of DFOB to the pre-existing Fe-$SRFA_1$ and Fe-$SRFA_2$ complexes to form a ternary complex, k_2 and k_4 are the kinetic rate constants of the release of the DFOB complex from the ternary complex and k_5 and k_6 are the kinetic rate constant of the release of SRFA from the ternary complex to yield the Fe-DFOB binary complex. Irreversibility over a time period of many hours implies very slow dissociation of the ternary complex, i.e.: small k_5 and k_6. We fixed k_5 and k_6 to the published value of 1.5×10^{-6} s^{-1} for the dissociation of Fe-DFOB complexes (Witter et al., 2000).

The mechanism explains the same decrease of the Fe-SRFA concentration found when the SRFA binding groups are fully or partially saturated (Figs. 1 and 2 and section 4.3) as the iron-free SRFA lacks the ability to compete with the irreversibly bound Fe-DFOB complexes.

The kinetic rates and conditional equilibrium constants produced by fitting the data in Figs. 1 and 4 to the model described in Eqs. 8 and 9 can be found in Table 1. The quality of fitting of the selected mechanism and kinetic rate constants in Table 1 to the experimental data can be examined in Fig. 8. Overall, the dissociation and formation kinetic rate constants of the slowly dissociating Fe-$SRHS_1$ complexes tend to decrease as the concentration of DFOB increases, presumably due to the labilization of higher iron affinity moieties, while the kinetic rate

Table 1
Kinetic rate constants obtained from fitting the data shown in Figs. 1 and 4 according to the reaction mechanism described by Eqs. 8 and 9. Irreversibility in the time scale of the study was achieved by setting k_3 and k_6 to a value of 1.5 10^{-6} s^{-1}.

[DFOB] (nM)	k_1 (10^4 $M^{-1}\cdot s^{-1}$)	k_2 (10^{-4} s^{-1})	k_3 (10^4 $M^{-1}\cdot s^{-1}$)	k_4 (10^{-4} s^{-1})
		1 mg SRFA L^{-1}		
+ 15	18.1 ± 4.7	117 ± 31	1.85 ± 0.03	0.772 ± 0.027
+ 30	6.50 ± 0.89	50.0 ± 7.5	1.56 ± 0.04	0.686 ± 0.031
+ 50	5.56 ± 5.28	6.39 ± 5.56	0.94 ± 5.28	~0*
		1 mg SRHA L^{-1}		
+ 35	0.627 ± 0.025	2.10 ± 0.08	5.94 ± 0.61	54.4 ± 6.4
+ 70	0.625 ± 0.025	3.86 ± 0.14	7.22 ± 3.89	169 ± 94
+ 100	0.168 ± 0.007	1.46 ± 0.06	4.17**	64.4 ± 1.7
+ 120	0.142 ± 0.003	0.639 ± 0.018	2.56 ± 0.14	39.6 ± 2.4
+240	0.075 ± 0.001	0.406 ± 0.011	18.44 ± 0.11	43.9 ± 2.8

* value 3 orders of magnitude lower than the other two k_4,
** value had to be fixed to achieve convergence.

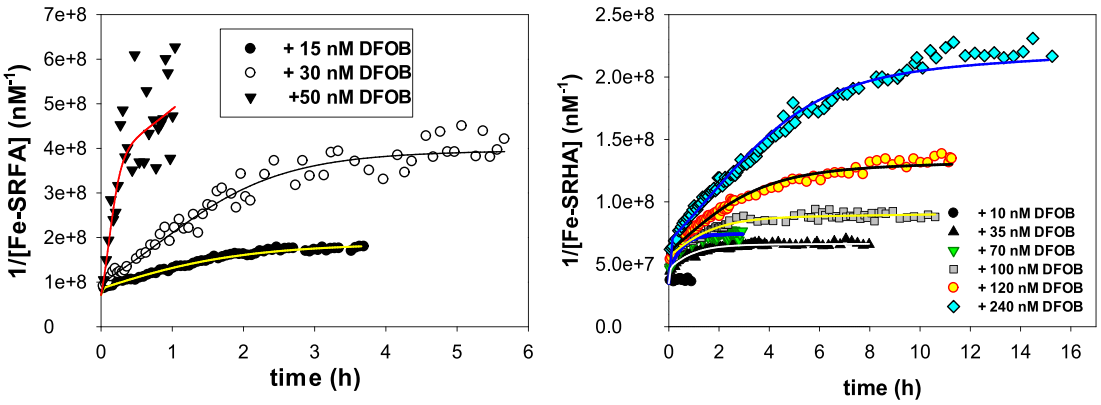

Fig. 8. Characteristic plot of second-order kinetics for all data shown in Figs. 1 and 4. Lines are the result of modelling the kinetic data according to the associative irreversible mechanism with two types of SRHS binding sites shown in Eqs. 8 and 9.

constants of the fast dissociating Fe-SRHS$_2$ complexes did not show any significant trend.

4.10. Formation of organic-organic bonds or ternary species

A further source of deviation from the D and A mechanisms shown in Eqs. 5 to 7 can be introduced through the formation of complexes in which both ligands are present. This could occur by formation of ternary complexes (A mechanism) that do not dissociate at the equilibrium, direct L-L binding or binding of a ligand to non-binding components of the DOM (L-DOM). Consequently, the binding ability of a fraction of the binding moieties of one or both ligands could be modified or even compromised. Unfortunately for the sake of simplicity, organic-organic interactions in the environment are common. HS, characterized by their hydrophobicity, form adducts with many other hydrophobic ligands via π–π interactions, hydrophobic effect and hydrogen bonding (Chianese et al., 2020). DFOB-organic interactions involving hydroxamate and non-binding functional groups are common in nature as a strategy to facilitate membrane transport (see (Crumbliss and Harrington, 2009) and references therein).

The binding of HS to DFOB has been verified by NMR spectroscopy and pyrolysis-GC-MS techniques (Higashi et al., 1998) and by using FTIR spectroscopy in the presence of iron at pH 6.5 (Stewart et al., 2013). However, NMR and FTIR spectroscopy techniques require concentrations many orders of magnitude higher than those found in seawater. It cannot be concluded that at natural concentrations, ligand–ligand complexes will form at concentrations enough to significantly interfere with our calculations.

Despite knowing in advance that our CSV method could not produce unambiguous evidence for ternary complex formation, we explored the presence or absence of deviations from the known behaviour of binary systems in an experiment with iron in excess of the combined concentration of SRFA and DFOB. Important considerations are that:

- the CSV signal is exclusively created by the adsorption of the Fe-HS complex on the HMDE and electrochemical reduction of Fe(III) (Laglera et al., 2007), without contribution from Fe-DFOB complexes (Spasojevic et al., 1999),
- iron-free HS can adsorb onto the HMDE but do not give any CSV signal (Laglera et al., 2007),
- under iron in excess, all ligands are saturated and changes in the CSV signal cannot be caused by net ligand exchange but formation of adducts.

However, there are three possible sources of uncertainty for our experimental design that could impede a correct interpretation of the CSV signals:

- if SRHS-Fe-DFOB complexes are generated and maintain the hydrophobic nature of HS, potentially adsorbing onto the HMDE, there is a hypothetical possibility of producing a CSV signal. This will depend on whether the Fe-DFOB complex reacts (and therefore labilizes) an iron-binding group of SRFA, resulting in a decrease of the CSV signal, or a non-binding group, leading to a CSV signal increase. Either way, it should be pointed out once again that no electrolabile ternary complex was formed in our experiments, even after many hours (Fig. 7), when DFOB was saturated with iron before the addition of iron-free SRFA'. Therefore, to experimentally verify the formation of ternary complexes, for example using spectroscopic techniques such as X-ray absorption spectroscopy, it is necessary that DFOB is added in its uncomplexed form.

For this experiment, 10 mL aliquots of UV seawater were sequentially spiked first with 2 mg SRFA L^{-1} or 1 mg SRHA L^{-1}, then with DFOB for a concentration in the range of 0 to 100 nM DFOB for SRFA, or 0 to 300 nM DFOB for SRHA and finally 600 nM Fe. All samples were equilibrated overnight at room temperature before the first measurement with the aim to complete the precipitation of iron before analysis. We did not observe any changes in the CSV peak within the 30 min period required to complete five analyses, indicating that the overnight period was sufficient to complete the precipitation of excess iron. The Fe-SRFA signal increased by a factor of about 1.2 with the added concentration of DFOB until it reached an apparent maximum after the addition of 30 nM DFOB (Fig. 9). This result would support the possible electrolabilization of the Fe-DFOB complexes through the formation of ternary Fe-DFOB-SRFA complexes. In the case of SRHA, the CSV signal decreased with the DFOB concentration reaching 80 % of the initial signal at DFOB concentrations between 100 and 200 nM. At a DFOB addition of 300 nM, the Fe-SRHA signal increased, although we would need better resolution to confirm such recovery at higher DFOB concentrations.

In the absence of spectroscopic evidence, we can only hypothesize about the processes that could explain this behaviour. Firstly, the higher iron contamination of the SRHA standard could have prevented the interaction of DFOB with the key iron complexing moieties of the SRHA. Secondly, co-precipitation of iron and Fe-SRHA complexes could partially explain the decrease of the CSV signal. HA molecules are larger and more hydrophobic than FA molecules and should be more prone to processes such as flocculation. This preferential precipitation of higher molecules has been observed in salinity gradients (Aftab and Hur, 2017; Linkhorst et al., 2017). Thirdly, we cannot rule out that DFOB may cause conformational changes in SRHA molecules or decrease the hydrophobicity of ternary complexes by reducing their affinity to adsorb onto the HMDE during the analytical accumulation step.

If any of the hypothesis presented above is confirmed on a significant

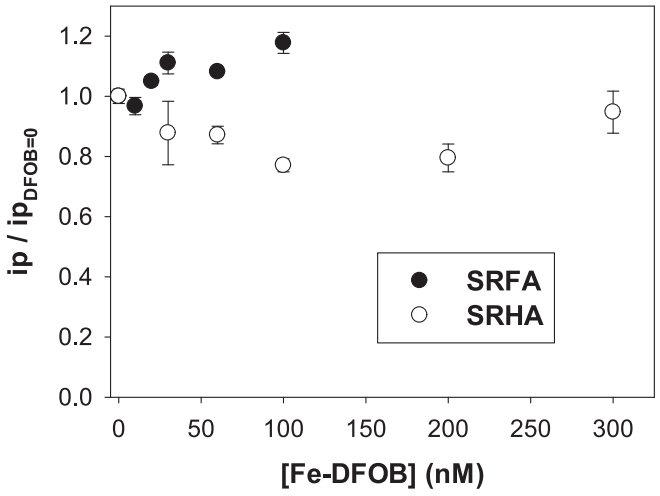

Fig. 9. B) CSV signal obtained in seawater after the addition of 2 mg/L SRFA and 1 mg/L SRHA, different concentrations of DFOB and Fe in excess of the combined ligand concentrations, allowing equilibration overnight before analysis. Error bars are the standard deviation of four CSV measurements in the same aliquot.

scale, it is possible that the estimation of HS binding affinity, including this study, may have been biased in CLE experiments (sections 4.2 to 4.5). Firstly, if the binding ability of any of the DFOB hydroxamate groups was compromised by non-binding SRHS or iron-free binding SRHS generated during the kinetic phase, we could have overestimated the $K'_{Fe'\text{-}SRHS}$. Secondly, direct interactions between SRHS and DFOB could have altered or impeded binding by SRHS resulting in either over- or underestimation of $K'_{Fe'\text{-}SRHS}$, depending on whether the hydroxamate groups, the terminal non-iron binding terminal amine of the siderophore, or both were involved. To shed more light on the interactions between the components of the Fe/SRHS/DFOB system at natural concentrations, the development of spectroscopic techniques suited for lower concentrations would be necessary.

The confirmation of strong interactions between HS and other ligands (via simultaneous Fe binding or direct L-L interaction) at the nanomolar and subnanomolar natural concentrations of Fe, HS, and other ligands in seawater would hold profound geochemical implications. Siderophores could integrate into colloids (Lin et al., 2020), co-precipitate with Fe and HS during estuarine trapping (resulting in their incorporation into coastal sediments) (Batchelli et al., 2010), and become associated with fractions with hydrophobicity, size, or net charge different from their properties when dissolved in seawater in isolation.

5. Implications for the study of iron cycling in seawater

5.1. Contribution of humic iron to the iron cycle

Humic iron is possibly the main source of iron in estuarine and coastal waters (Krachler et al., 2015) and probably contributes decisively to the iron pool in vast areas of the open ocean (Laglera et al., 2019; Muller, 2018). Our electrochemical method is currently unique in allowing the calculation of HS concentrations after calibration with SRFA and their contribution to the iron ligand pool prior to knowledge of their iron BC. The range of published HS concentrations in open ocean waters expands from near the detection limit (0.005 mg SRFA L^{-1}) to many tenths of mg SRFA L^{-1}, equivalent to humic ligand concentrations of tens of pM to around 1 nM Fe (Dulaquais et al., 2018; Laglera and van den Berg, 2009; Mellett and Buck, 2020; Slagter et al., 2019). This is below or close to the ligand concentrations found in the ocean, which would make HS the main contributor to the pool of organic ligands in some water masses. The limited iron ligand exchange of Fe-HS complexes with other ligands predicted from our $K'_{Fe'\text{-}DFOB}/K'_{Fe'\text{-}SRHS}$ ratios, it is not just a change of paradigm, it is also important in terms of iron bioavailability. The formation of HS complexes increases iron bioavailability (Chen and Wang, 2008) not only because of iron exchange with cell membrane functional group, but also because HS chromophores in the euphotic layer are prone to participate in the reduction of Fe(III) into the more bioavailable Fe(II) (Fujii et al., 2010). The high stability of Fe-HS complexes concurs with the prevalence of humic iron (~80 % of DFe) found in HS-rich surface waters of the Arctic Transpolar Drift despite months to years of residence under ice (Laglera et al., 2019; Slagter et al., 2019) and the residual humic iron (0–20 % DFe) concentrations found in HS-poor waters of blooming surface waters over the Brazilian coast shelf (Sukekava et al., 2023).

5.2. Understanding the partitioning of iron between different ligands

The low concentration and large heterogeneity of oceanic DOM have prevented the identification of individual contributors to the pool of iron ligands in the ocean. Our results provide a biochemical and ecological sense of the relative concentrations of the different ligands found so far in ocean waters.

Recent advances in HPLC-MS techniques have allowed for the detection of combined siderophore concentrations ranging from units to tens of pmol/L across various marine regions. These concentrations are found to be one to two orders of magnitude lower than those reported for L and HS ligand concentrations in oceanic waters. (Boiteau et al., 2016; Boiteau et al., 2019; Bundy et al., 2018; Gledhill et al., 2022). These low concentrations imply that siderophore consumption processes such as photodegradation (Barbeau et al., 2003), prokaryotic uptake (Hopkinson and Barbeau, 2012) and scavenging (Hogle et al., 2022) shorten their half-life in the ocean sufficiently to prevent their accumulation. The involvement of Fe-siderophore complexes in chemical reactions with time scales significantly longer than their residence time in the ocean would be of negligible environmental significance. Ligand exchange rates such as those obtained in this study and dissociation rate constants leading to half-lives of the order of months such as those found for the hydroxamate siderophores desferrioxamine E and ferrichrome and extracted amphibactins by iron isotope exchange in seawater (Boiteau and Repeta, 2022) could be considered irreversible from an ecological perspective.

The $K'_{Fe'\text{-}DFOB}/K'_{Fe'\text{-}SRHS}$ ratios we report here and the use of Eq. S5 indicate that at natural HS:siderophore concentration ratios, the contribution of siderophores to iron complexation at equilibrium would be residual. However, the irreversibility of iron-siderophore complexation in competition with HS describes a situation where iron speciation closely adheres to a “first come, first served” principle: siderophore concentrations one to two orders of magnitude lower than HS concentrations would struggle to effectively sequester significant concentrations of iron bound to HS; conversely, iron bound to a siderophore would not be sequestered by HS.

It is crucial to understand that, in the light of our results, small concentrations of exuded siderophores can satisfy the iron requirements of the prokaryotic fraction assimilating Fe-siderophore complexes. Accumulating siderophores in the water column at nanomolar concentrations to compete with other ligands is not feasible because prokaryotes would need to bear the high cost of synthesizing and exuding energy-consuming siderophores (Völker and Wolf-Gladrow, 1999). According to our $K'_{Fe'\text{-}DFOB}/K'_{Fe'\text{-}SRHS}$ ratios, picomolar concentrations of Fe-siderophore complexes would be overcompeted by HS failing to hold any significant iron concentration. However, the lack of reversibility of Fe-siderophore complexes by HS implies that small concentrations of siderophores in the water column maintain the Fe-siderophore requirements of prokaryote communities.

Our $K'_{Fe'\text{-}DFOB}/K'_{Fe'\text{-}SRHS}$ ratios also explain the recent discovery using clean HPLC-MS techniques of iron saturated siderophores in coastal

waters that in open ocean waters were approximately 40 % iron-free despite DFe concentrations two orders of magnitude above the combined concentration of siderophores (Boiteau et al., 2016). Coastal waters contain iron-saturated siderophores from freshwater supplies (Maknun et al., 2023) and autochthonous siderophores can compete with the iron oxyhydroxide forms common in riverine and upwelling sources. However, fresh iron-free siderophores released in open ocean waters have to sequester iron from DOM complexes (including HS), which are present in much higher concentrations.

However, in deep waters, the lack of capacity of HS to sequester iron bound to other natural ligands (such as hexadentate siderophores) could be behind the low iron saturation of HS (15–20 %) found at a deep Arctic Ocean station (Laglera et al., 2019). Siderophores in deep waters are released during microbial remineralization of POC (and thus iron), which would facilitate the direct binding of iron to siderophores. The strong correlation observed between the vertical profiles of DFe and fluorescent DOM in deep ocean waters gave rise to the hypothesis that HS may regulate iron solubility at depth (Kitayama et al., 2009). Recent developments that allow the estimation of the concentration of iron bound to HS (Sukekava et al., 2018) warrant further studies to verify or challenge the controlling role of HS in deep-sea iron speciation. However, studies in deep waters are currently limited by the absence of HS standards that could better represent autochthonous HS production.

Our description of the competition between siderophores and HS closely aligns with the modeling based on field measurements of siderophores recently published by Gledhill and coauthors (Gledhill et al., 2022).

From an analytical point of view, it can be expected that in a “first come, first served” complexation scenario, the reversibility of iron complexes, the order of reagent addition and the presence of accelerators prior to analysis could impact the results of CLE-CSV analysis. Moreover, if the presence of ternary siderophore-Fe-HS complexes in seawater is confirmed, the conventional use of three terms mass balances (Eq. S3) would introduce significant bias for the estimation of $K'_{Fe'L}$. The implications for the reliability of speciation models could be serious. The existence of ternary and ligand–ligand complexes could also affect HPLC extraction and MS analysis as adducts may exhibit different chemical reactivity on the column, and the m/z ratio of an undetermined fraction of siderophores could be substantially altered.

6. Conclusions

We are beginning to understand the real role of HS in the solubility and transport of iron from terrestrial sources. The chemical characteristics of HS present a drawback for their analysis by HPLC-MS and the determination of their complexing parameters by CLE-AdCVS, although they allow their direct determination at natural concentrations by AdCSV of their iron complexes. We took advantage of this electrolability to monitor the kinetics of iron ligand exchange up to equilibrium when iron from Fe-HS complexes is sequestered by the siderophore DFOB and other complexes in the nanomolar range. We established that the segmented kinetics we observed is evidence of the heterogeneity of the HS binding groups although a fraction of the ligand exchange is severely accelerated by the effect of the major divalent cations in seawater. Partitioning at the equilibrium showed that, contrary to the current paradigm, HS have, on average, a similar affinity for iron as DFOB, corroborating previous observations showing that the affinity of HA for iron is higher than that of FA. However, when iron is bound to hexadentate ligands, this complexation is inert to competition from the large molecules of HS. This irreversibility, in combination with the different ligand exchange kinetics we observed using PP IX and EDTA as competing ligands, indicates that iron exchange between HS and DFOB is associative. Our experiments suggest that a small but significant concentration of the ternary complex or a ligand–ligand complex could be stable at equilibrium.

Our findings explain the discovery of a significant fraction of ocean siderophores found in their iron-free form, the high concentrations of strong ligands found in HS-rich waters or the problems encountered with the study of HS complexation of iron by CLE-AdCSV techniques.

Studies under saturation of all ligands point to the presence of small but significant concentrations of complexes where ligand to ligand interactions could change the physicochemical and or binding (log K') characteristics of the iron complexes when mixed in seawater. Consequently, the ratios of reagents in CLE studies and the sequential order of reagent addition are essential in CLE experiments.

Data availability

Experimental data and Dynafit software scripts are available through Zenodo. At 909 https://doi.org/10.5281/zenodo.8047795.

Declaration of competing interest

The authors declare that they have no known competing financial interests or personal relationships that could have appeared to influence the work reported in this paper.

Acknowledgements

We want to thank Loes Gerringa and Antonio Costa for their insightful comments during the preparation of the manuscript. CS participated thanks to a grant provided by the Coordenação de Aperfeiçoamento de Pessoal de Nível Superior (CAPES, 88882.182291/2007-01). LML acknowledges financial support from project PID2020-115291GB-I00, funded by MCIN/AEI/10.13039/501100011033/ and project CTM2017-84763-C3-3-R, funded by MCIN/AEI/10.13039/501100011033/ and FEDER. JD thanks the Government of the Balearic Islands, Conselleria d’Innovació, Recerca i Turisme for his PhD scholarship (no. FPI/2034/2017).

Appendix A. Supplementary material

The Supplementary Material includes i) some experimental and modelled kinetics that support the text but are not essential to its understanding, ii) a description of the analytical problems we found during our experimental, their source and the limitations that suppose for interpretation and iii) a brief description of the mechanistic models of iron ligand exchange used in this work with the definition of the kinetic rate constants and the number of chemical species used to fit kinetic data for each mechanism. Supplementary material to this article can be found online at https://doi.org/10.1016/j.gca.2023.12.007.

References

Abualhaija, M.M., van den Berg, C.M.G., 2014. Chemical speciation of iron in seawater using catalytic cathodic stripping voltammetry with ligand competition against salicylaldoxime. Mar. Chem. 164, 60–74.

Aftab, B., Hur, J., 2017. Fast tracking the molecular weight changes of humic substances in coagulation/flocculation processes via fluorescence EEM-PARAFAC. Chemosphere 178, 317–324.

Barbeau, K., Rue, E.L., Trick, C.G., Bruland, K.W., Butler, A., 2003. Photochemical reactivity of siderophores produced by marine heterotrophic bacteria and cyanobacteria based on characteristic Fe(III) binding groups. Limnol. Oceanogr. 48, 1069–1078.

Batchelli, S., Muller, F.L.L., Chang, K.-C., Lee, C.-L., 2010. Evidence for strong but dynamic iron-humic colloidal associations in humic-rich coastal waters. Environ. Sci. Technol. 44, 8485–8490.

Boguta, P., D'Orazio, V., Senesi, N., Sokołowska, Z., Szewczuk-Karpisz, K., 2019. Insight into the interaction mechanism of iron ions with soil humic acids. The effect of the pH and chemical properties of humic acids. J. Environ. Manage. 245, 367–374.

Boiteau, R.M., Mende, D.R., Hawco, N.J., McIlvin, M.R., Fitzsimmons, J.N., Saito, M.A., Sedwick, P.N., DeLong, E.F., Repeta, D.J., 2016. Siderophore-based microbial adaptations to iron scarcity across the eastern Pacific Ocean. Proc. Natl. Acad. Sci. U. S.A. 113, 14237–14242.

Boiteau, R.M., Repeta, D.J., 2022. Slow kinetics of iron binding to marine ligands in seawater measured by isotope exchange liquid chromatography-inductively coupled plasma mass spectrometry. Environ. Sci. Technol. 56, 3770–3779.

Boiteau, R.M., Till, C.P., Coale, T.H., Fitzsimmons, J.N., Bruland, K.W., Repeta, D.J., 2019. Patterns of iron and siderophore distributions across the California Current System. Limnol. Oceanogr. 64, 376–389.
Buck, K.N., Sohst, B., Sedwick, P.N., 2015. The organic complexation of dissolved iron along the U.S. GEOTRACES (GA03) North Atlantic Section. Deep Sea Res. Part II: Topical Stud. Oceanogr. 116, 152–165.
Bundy, R.M., Boiteau, R.M., McLean, C., Turk-Kubo, K.A., McIlvin, M.R., Saito, M.A., Van Mooy, B.A.S., Repeta, D.J., 2018. Distinct Siderophores Contribute to Iron Cycling in the Mesopelagic at Station ALOHA. Front. Mar. Sci. 5, 61.
Chen, M., Wang, W.-X., 2008. Accelerated uptake by phytoplankton of iron bound to humic acids. Aquat. Biol. 3, 155–166.
Chianese, S., Fenti, A., Iovino, P., Musmarra, D., Salvestrini, S., 2020. Sorption of organic pollutants by humic acids: a review. Molecules 25.
Croot, P.L., Johansson, M., 2000. Determination of iron speciation by cathodic stripping voltammetry in seawater using the competing ligand 2-(2-thiazolylazo)-p-cresol (TAC). Electroanalysis 12, 565–576.
Crumbliss A.L., Harrington J.M., 2009. Iron sequestration by small molecules: Thermodynamic and kinetic studies of natural siderophores and synthetic model compounds. Advances in Inorganic Chemistry, Vol 61: Metal Ion Controlled Reactivity **61**, 179-250.
Dulaquais, G., Waeles, M., Gerringa, L.J.A., Middag, R., Rijkenberg, M.J.A., Riso, R., 2018. The biogeochemistry of electroactive humic substances and its connection to iron chemistry in the North East Atlantic and the Western Mediterranean Sea. J. Geophys. Res. Oceans 123, 5481–5499.
Fox, L.E., Wofsky, S.C., 1983. Kinetics of removal of iron colloids from estuaries. Geochim. Cosmochim. Acta 47, 211–216.
Fujii, M., Rose, A.L., Waite, T.D., Omura, T., 2008. Effect of divalent cations on the kinetics of Fe(III) complexation by organic ligands in natural waters. Geochim. Cosmochim. Acta 72, 1335–1349.
Fujii, M., Rose, A.L., Waite, T.D., Omura, T., 2010. Oxygen and superoxide-mediated redox kinetics of iron complexed by humic substances in coastal seawater. Environ. Sci. Technol. 44, 9337–9342.
Gerringa, L.J.A., Rijkenberg, M.J.A., Thuróczy, C.E., Maas, L.R.M., 2014. A critical look at the calculation of the binding characteristics and concentration of iron complexing ligands in seawater with suggested improvements. Environ. Chem. 11, 114–136.
Gerringa, L.J.A., Gledhill, M., Ardiningsih, I., Muntjewerf, N., Laglera, L.M., 2021. Comparing CLE-AdCSV applications using SA and TAC to determine the Fe-binding characteristics of model ligands in seawater. Biogeosci. 18, 5265–5289.
Gledhill, M., 2001. Electrospray ionisation-mass spectrometry of hydroxamate siderophores. Analyst 126, 1359–1362.
Gledhill, M., Buck, K.N., 2012. The organic complexation of iron in the marine environment: a review. Front. Microbiol. 3, 1–19.
Gledhill, M., Zhu, K., Rusiecka, D., Achterberg, E.P., 2022. Competitive interactions between microbial siderophores and humic-like binding sites in European shelf sea waters. Front. Mar. Sci. 9, 855009.
Heerah, K.M., Reader, H.E., 2022. Towards the identification of humic ligands associated with iron transport through a salinity gradient. Sci. Rep. 12, 15545.
Helm, L., Merbach, A.E., 2005. Inorganic and bioinorganic solvent exchange mechanisms. Chem. Rev. 105, 1923–1959.
Hering, J.G., Morel, F.M.M., 1988. Humic-acid complexation of calcium and copper. Environ. Sci. Technol. 22, 1234–1237.
Higashi, R.M., Fan, T.-W.-M., Lane, A.N., 1998. Association of desferrioxamine with humic substances and their interaction with cadmium (II) as studied by pyrolysis-gas chromatography-mass spectrometry and nuclear magnetic resonance spectroscopy. Analyst 123, 911–918.
Hogle, S.L., Hackl, T., Bundy, R.M., Park, J., Satinsky, B., Hiltunen, T., Biller, S., Berube, P.M., Chisholm, S.W., 2022. Siderophores as an iron source for picocyanobacteria in deep chlorophyll maximum layers of the oligotrophic ocean. ISME J. 16, 1636–1646.
Hopkinson, B.M., Barbeau, K.A., 2012. Iron transporters in marine prokaryotic genomes and metagenomes. Environ. Microbiol. 14, 114–128.
Kitayama, S., Kuma, K., Manabe, E., Sugie, K., Takata, H., Isoda, Y., Toya, K., Saitoh, S.-I., Takagi, S., Kamei, Y., Sakaoka, K., 2009. Controls on iron distributions in the deep water column of the North Pacific Ocean: Iron(III) hydroxide solubility and marine humic-type dissolved organic matter. J. Geophys. Res. Oceans 114, C08019.
Kogut, M.B., Voelker, B.M., 2001. Strong copper-binding behavior of terrestrial humic substances in seawater. Environ. Sci. Technol. 35, 1149–1156.
Krachler, R., Krachler, R.F., Wallner, G., Hann, S., Laux, M., Cervantes Recalde, M.F., Jirsa, F., Neubauer, E., von der Kammer, F., Hofmann, T., Keppler, B.K., 2015. River-derived humic substances as iron chelators in seawater. Mar. Chem. 174, 85–93.
Krachler, R., Krachler, R., Valda, A., Keppler, B.K., 2019. Natural iron fertilization of the coastal ocean by "blackwater rivers". Sci. Total Environ. 656, 952–958.
Kuhn, K.M., Maurice, P.A., Neubauer, E., Hofmann, T., von der Kammer, F., 2014. Accessibility of Humic-Associated Fe to a Microbial Siderophore: Implications for Bioavailability. Environ. Sci. Technol. 48, 1015–1022.
Kuzmič, P., 1996. Program DYNAFIT for the analysis of enzyme kinetic data: application to HIV proteinase. Anal. Biochem. 237, 260–273.
Laglera, L.M., Filella, M., 2015. The relevance of ligand exchange kinetics in the measurement of iron speciation by CLE–AdCSV in seawater. Mar. Chem. 173, 100–113.
Laglera, L.M., Battaglia, G., van den Berg, C.M.G., 2007. Determination of humic substances in natural waters by cathodic stripping voltammetry of their complexes with iron. Anal. Chim. Acta 599, 58–66.
Laglera, L.M., Battaglia, G., van den Berg, C.M.G., 2011. Effect of humic substances on the iron speciation in natural waters by CLE/CSV. Mar. Chem. 127, 134–143.
Laglera, L.M., Santos-Echeandía, J., Caprara, S., Monticelli, D., 2013. Quantification of iron in seawater at the low picomolar range based on optimization of bromate/ammonia/dihydroxynaphtalene system by catalytic adsorptive cathodic stripping voltammetry. Anal. Chem. 85, 2486–2492.
Laglera, L.M., Tovar-Sánchez, A., Iversen, M.H., González, H.E., Naik, H., Mangesh, G., Assmy, P., Klaas, C., Mazzocchi, M.G., Montresor, M., Naqvi, S.W.A., Smetacek, V., Wolf-Gladrow, D.A., 2017. Iron partitioning during LOHAFEX: copepod grazing as a major driver for iron recycling in the Southern Ocean. Mar. Chem. 196, 148–161.
Laglera, L.M., Sukekava, C., Slagter, H.A., Downes, J., Aparicio-Gonzalez, A., Gerringa, L.J.A., 2019. First quantification of the controlling role of humic substances in the transport of iron across the surface of the Arctic Ocean. Environ. Sci. Technol. 53, 13136–13145.
Laglera, L.M., Tovar-Sanchez, A., Sukekava, C.F., Naik, H., Naqvi, S.W.A., Wolf-Gladrow, D.A., 2020. Iron organic speciation during the LOHAFEX experiment: iron ligands release under biomass control by copepod grazing. J. Mar. Syst. 207, 103151.
Laglera, L.M., van den Berg, C.M.G., 2009. Evidence for geochemical control of iron by humic substances in seawater. Limnol. Oceanogr. 54, 610–619.
Lin, P., Xu, C., Sun, L., Xing, W., Santschi, P.H., 2020. Incorporation of hydroxamate siderophore and associated Fe into marine particles in natural seawater. Front. Mar. Sci. 7, 584628.
Linkhorst, A., Dittmar, T., Waska, H., 2017. Molecular fractionation of dissolved organic matter in a shallow subterranean estuary: the role of the iron curtain. Environ. Sci. Technol. 51, 1312–1320.
Liu, X.W., Millero, F.J., 1999. The solubility of iron hydroxide in sodium chloride solutions. Geochim. Cosmochim. Acta 63, 3487–3497.
Liu, X.W., Millero, F.J., 2002. The solubility of iron in seawater. Mar. Chem. 77, 43–54.
Maknun, L., Kińska, K., González-Álvarez, I., Ouerdane, L., Lauga, B., Siripinyanond, A., Szpunar, J., Lobinski, R., 2023. Quantitative determination of iron-siderophore complexes in peat by isotope-exchange size-exclusion UPLC–Electrospray Ionization High-Resolution Accurate Mass (HRAM) mass spectrometry. Anal. Chem. 95, 9182–9190.
Mellett, T., Buck, K.N., 2020. Spatial and temporal variability of trace metals (Fe, Cu, Mn, Zn Co, Ni, Cd, Pb), iron and copper speciation, and electroactive Fe-binding humic substances in surface waters of the eastern Gulf of Mexico. Mar. Chem. 227, 103891.
Morel, F.M.M., Hering, J.G., 1993. Principles and applications of aquatic chemistry. John Wiley & Sons.
Muller, F.L.L., 2018. Exploring the potential role of terrestrially derived humic substances in the marine biogeochemistry of iron. Front. Earth Sci. 6, 159.
Muller, F.L.L., Batchelli, S., 2013. Copper binding by terrestrial versus marine organic ligands in the coastal plume of River Thurso, North Scotland. Estuar. Coast. Shelf Sci. 133, 137–146.
Oldham, V.E., Miller, M.T., Jensen, L.T., Luther Iii, G.W., 2017. Revisiting Mn and Fe removal in humic rich estuaries. Geochim. Cosmochim. Acta 209, 267–283.
Rose, A.L., Waite, T.D., 2003. Kinetics of iron complexation by dissolved natural organic matter in coastal waters. Mar. Chem. 84, 85–103.
Rue, E.L., Bruland, K.W., 1995. Complexation of iron(III) by natural organic ligands in the Central North Pacific as determined by a new competitive ligand equilibration/adsorptive cathodic stripping voltammetric method. Mar. Chem. 50, 117–138.
Schijf, J., Burns, S.M., 2016. Determination of the side-reaction coefficient of Desferrioxamine B in trace-metal-free seawater. Front. Mar. Sci. 3, 117.
Scolaro, L.M., Castriciano, M., Romeo, A., Patanè, S., Cefalì, E., Allegrini, M., 2002. Aggregation behavior of Protoporphyrin IX in aqueous solutions: clear evidence of vesicle formation. J. Phys. Chem. B 106, 2453–2459.
Shaked, Y., Buck, K.N., Mellett, T., Maldonado, M.T., 2020. Insights into the bioavailability of oceanic dissolved Fe from phytoplankton uptake kinetics. ISME J. 14, 1182–1193.
Sholkovitz, E.R., 1978. The flocculation of dissolved Fe, Mn, Al, Cu, Ni, Co and Cd during estuarine mixing. Earth. Planet. Sci. Lett. 41, 77–86.
Slagter, H.A., Laglera, L.M., Sukekava, C., Gerringa, L.J.A., 2019. Fe-binding organic ligands in the humic-rich transpolar drift in the surface arctic ocean using multiple voltammetric methods. J. Geophys. Res. Oceans 124, 1491–1508.
Spasojevic, I., Armstrong, S.K., Brickman, T.J., Crumbliss, A.L., 1999. Electrochemical behavior of the Fe(III) complexes of the cyclic hydroxamate siderophores alcaligin and desferrioxamine E. Inorg. Chem. 38, 449–454.
Stewart, A.G., Hudson-Edwards, K.A., Dubbin, W.E., 2013. Mechanisms of goethite dissolution in the presence of desferrioxamine B and Suwannee River fulvic acid at pH 6.5. Geochim. Cosmochim. Acta 115, 1–14.
Stockdale, A., Tipping, E., Hamilton-Taylor, J., Lofts, S., 2011. Trace metals in the open oceans: speciation modelling based on humic-type ligands. Environ. Chem. 8, 304–319.
Sukekava, C.F., Downes, J., Slagter, H.A., Gerringa, L.J.A., Laglera, L.M., 2018. Determination of the contribution of humic substances to iron complexation in seawater by catalytic cathodic stripping voltammetry. Talanta 189, 359–364.
Sukekava, C.F., Andrade, C.F.F.d., Niencheski, L.F.H., de Souza, M.S., Laglera, L.M., 2023. Macronutrients, iron and humic substances summer cycling over the extended continental shelf of the South Brazil Bight. Sci. Total Environ. 865, 161182.
Tipping, E., Hurley, M.A., 1992. A unifying model of cation binding by humic substances. Geochim. Cosmochim. Acta 56, 3627–3641.
van den Berg, C.M.G., 1995. Evidence for organic complexation of iron in seawater. Mar. Chem. 50, 139–157.
Völker, C., Wolf-Gladrow, D.A., 1999. Physical limits on iron uptake mediated by siderophores or surface reductases. Mar. Chem. 65, 227–244.
Whitby, H., Bressac, M., Sarthou, G., Ellwood, M.J., Guieu, C., Boyd, P.W., 2020a. Contribution of electroactive humic substances to the iron-binding ligands released

during microbial remineralization of sinking particles. Geophys. Res. Lett. 47, e2019GL086685.
Whitby, H., Planquette, H., Cassar, N., Bucciarelli, E., Osburn, C.L., Janssen, D.J., Cullen, J.T., González, A.G., Völker, C., Sarthou, G., 2020b. A call for refining the role of humic-like substances in the oceanic iron cycle. Sci. Rep. 10, 1–12.
Wilkins, R.G., 1991. Substitution reactions, in: GmbH&Co., W.-V.V. (Ed.), Kinetics and mechanism of reactions of transition metal complexes, Weinheim, pp. 200-246.
Witter, A.E., Hutchins, D.A., Butler, A., Luther, G.W., 2000. Determination of conditional stability constants and kinetic constants for strong model Fe-binding ligands in seawater. Mar. Chem. 69, 1–17.
Wu, J., Luther III, G.W., 1995. Complexation of Fe(III) by natural organic ligands in the Northwest Atlantic Ocean by a competitive ligand equilibration method and a kinetic approach. Mar. Chem. 50, 159–177.
Yang, R., Su, H., Qu, S., Wang, X., 2017. Capacity of humic substances to complex with iron at different salinities in the Yangtze River estuary and East China Sea. Sci. Rep. 7, 1381.